CHALMERS
UNIVERSITY OF TECHNOLOGY

High-Z Solutions for Shielding and Radiopacity

Master's thesis in Nuclear Science and Technology

INGER ANDREA LIEN HESBØL

Department of Chemistry and Chemical Engineering
CHALMERS UNIVERSITY OF TECHNOLOGY
Gothenburg, Sweden 2019

Master's thesis 2019:NN

High-Z Solutions for Shielding and Radiopacity

INGER ANDREA LIEN HESBØL

CHALMERS
UNIVERSITY OF TECHNOLOGY

Department of Chemistry and Chemical Engineering
Nuclear Chemistry
Chalmers University of Technology
Gothenburg, Sweden 2019

High-Z Solutions for Shielding and Radiopacity
INGER ANDREA LIEN HESBØL

Supervisor: Teodora Retegan, Department of Chemistry and Chemical Engineering
Examiner: Name, Department

Master's Thesis 2019:NN
Department of Chemistry and Chemical Engineering
Nuclear Chemistry
Chalmers University of Technology
SE-412 96 Gothenburg
Telephone +46 31 772 1000

Cover: PIA12348, Great Observatories Unique Views of the Milky Way, retrieved from NASA image database. [1]

Typeset in LaTeX
Printed by [Name of printing company]
Gothenburg, Sweden 2019

High-Z Solutions for Shielding and Radiopacity
INGER ANDREA LIEN HESBØL
Department of Chemistry and Chemical Engineering
Chalmers University of Technology

Abstract

The biggest concern for future space exploration beyond low earth orbit, from a radiation perspective is galactic cosmic radiation and solar particle events, due to lack of satisfactory shielding options. This thesis explore the possibility to use high-Z elements dissolved in water, as a possible shielding for space exploration. The idea is to combining it with the currently used liquid cooling and ventilation garment, or in future habitat design. The experiments were performed by irradiating samples of Fricke solution, encased within the high-Z shielding solution through different methods, and the dose was measured by Fricke dosimetry. The results for the used concentrations indicates that it is not viable to combine the high-Z shielding solution with the current liquid cooling and ventilation garment. However, it can be possible to used when covering larger surfaces, which could be a possibility for future habitat design, and further work on this topic.

Keywords: High-Z solution, Space, Spacesuit, Liquid Cooling and Ventilation Garment, Habitat, Fricke Dosimetry

Acknowledgements

I would like to thank:

Teodora Retegan, my supervisor, who gave me a interesting project and always had time to listen and discuss on how to proceed with the experiments.

Sefan Alard, my co-supervisor, who has been part of several talks of how to proceed with experiments.

Luis and Anna-Elina, helpful PhD students, which on several occasions has accompanied me down to the gamma laboratory.

Vera and Alejandro, my office and laboratory mates, for help with and double checking my chemistry related calculations when in doubt.

All the other people at Nuclear Chemistry, that has provided answers or guidance on different topics.

My family, my boyfriend and his family, for all help and support you have provided trough these two years. Along with fellow MSc students, and offline as well as online friends, for encouraging words helping me pull through the hard times when I wanted nothing else then dropping out.

Inger Andrea Lien Hesbøl, Gothenburg, 06 2019

Contents

List of Figures

List of Tables

Acronyms

ALARA	**A**s **L**ow **A**s **R**easonably **A**chievab
CCA	**C**ommunications **C**arrier **A**ssembly
CMEs	**C**oronal **M**ass **E**jections
CNR	**C**ontrast to **N**oice **R**atio
CT	**C**omputed **T**omography
EVA	**E**xtra**v**ehicular **A**ctivity
GCR	**G**alactic **C**osmic **R**adiation
GSO	**G**eo**s**ynchronous **O**rbit
HDPE	**H**high **D**ensity **P**oly**e**thylene
HEO	**H**igh **E**arth **O**rbit
HUT	**H**ard **U**pper **T**orso
IEVA	**I**ntra/**E**xtra**v**ehicular **A**ctivity
IONPs	**I**ron **O**xide **N**nano**p**articles
ISS	**I**nternational **S**pace **S**tation
IVA	**I**ntra**v**ehicular **A**ctivity
LCG	**L**iquid **C**ooling **G**arments
LCVG	**L**iquid **C**ooling and **V**entilation **G**arment
LEO	**L**ow **E**arth **O**rb
LTA	**L**ower **T**orso **A**ssembly
MRI	**M**agnetic **R**esonance **I**maging
NASA	**N**ational **A**eronautics and **S**pace **A**dministration
NMR	**N**uclear **M**agnetic **R**esonance
NPs	**N**ano**p**articles
PLSS	**P**rimary **L**ife **S**upport **S**ubsystem
SPEs	**S**olar **P**article **E**vents

1
Introduction

On December 1972, Apollo 17 returned to the earth following a 12 day missions to the Moon [2]. This mission was the last manned space mission to have gone beyond low earth orbit (LEO). Today manned space missions are primary intra/extravehicular activity (IEVA) related to the International Space Station (ISS) located in low earth orbit.

When considering radiation shielding for future space exploration beyond LEO, the largest concerns is galactic cosmic radiation (GCR) and solar particle events (SPEs), along with making sure astronauts are not exposed to more then yearly and career radiation limits set by e.g. National Aeronautics and Space Administration (NASA) [3]. Both space radiation and dose limits are discussed further later in this paper. Such future plans for space missions beyond LEO involves new missions to the Moon, but also Mars [4].

The thesis assignment was given by Theodora Retegan, Associate Professor, Chemistry and Chemical Engineering, Nuclear Chemistry/Industrial Materials Recycling at Chalmers University of Technology. All experiments where preformed with resources available at Nuclear Chemistry at Chalmers University of Technology. A Gammacell 220 ^{60}Co irradiation unit was used for irradiating samples, and a Lambda 25 UV/VIS spectrometer was used for analysing samples. The absorbed dose was determined using Fricke dosimetry.

It explores the radiopacity potential of several high-Z elements dissolved in water, for the potential use as radiation shielding for future space exploration beyond LEO. The thought is that it could be combined with the currently used liquid cooling and ventilation garments (LCVG) worn by astronauts under their space suits. Or in combination with future habitat designs.

Within the field of medicine a substantial amount of studies has been conducted, exploring several different solutions containing high-Z elements and their potential use in especially computed tomography (CT) [5, 6, 7]. However, within the field of space exploration the studies conducted utilizing different high-Z elements has primary focused on structural shielding [8, 9, 10], while studies related to the space suit and the LCVG focus on designs with different synthetic compounds and fibers, or fundamentally different designs of the LCVG, but which still utilizes water [11, 12, 13]. Thus, not adding any significant insight to the purpose of this thesis. Therefore, the focus has been the high-Z elements from the medical studies and the structural shielding in space exploration.

This thesis paper is divided into six chapters. Chapter 2 presents several studies within the field of medicine and space exploration which utilizes high-Z elements. Chapter 3 presents insightful theory related to space, dose and the utilized measuring technique. Chapter 4 presents the conducted experimental work, while chapter 5 presents the results. Chapter 6 presents the final conclusion following the results in chapter 5, and future possibilities.

2
Background

2.1 Medicine

Within the field of medical applications, high-Z solutions are administered to patients undergoing imagining procedures. These solutions are commonly known as contrast agents. Depending on the imaging technique, different features of the high-Z element is utilized to enhance the image quality, providing valuable aid when diagnosing patients.

2.1.1 Computed Tomography

In CT it is the different attenuation of x-rays in the various tissues that are utilized [7]. The degree of x-ray attenuation is presented in equation (3.1), found under chapter 3.1 Equations, where the photoelectric effect is the most prevalent factor of the mass attenuation coefficient (μ) [7]. This photoelectric effect is proportional to the atomic number to the power of three (Z^3) [7]. Thus, high-Z solutions are used as contrast agents to enhanced the image contrast, by amplifying the x-ray attenuation, this results in an improved ability to differentiate between tissues of similar density [5, 7]. This improvement is so valuable when diagnosing a patient, that these contrast agents are used despite the concerns for toxicity risks [5].

These contrast agents are administered to the patient intravenously or orally, and used when examining the vascular system or urinary and gastrointestinal tracks [5] [6]. The examinations are conducted with x-ray tube potential in the range 80 to 140kV, increasing with the size of the patient [5, 6]. This x-ray tube potential range results in a x-ray spectra from approximately 55 to over 110keV in mean energies, depending on the filtration of the x-ray tube [6].

The commercially used contrast agents for CT contain either iodine or barium [5, 6]. However several experiments have been conducted, investigating other high-Z solutions as options for CT contrast agent, due to undesired contrast reduction of iodine based contrast agents at high x-ray tube potentials, as well as the desire to lower the administered dose to patient.

Experiments preformed by FitzGerald et al. [5] explores several high-Z solutions as alternative to iodine based contrast agent for intravascular CT examinations, which can be utilized at high x-rays tube potentials, consistent with average-size to large adults, without the image contrast reduction. The experiments demonstrates that

barium, gadolinium, ytterbium and tantalum do not exhibit the same image contrast reduction as iodine. Of these, gadolinium based solution demonstrated the best image contrast improvement, followed by tantalum based solution. However, there are ongoing debates regarding whether gadolinium based solutions for a general CT examination is safe for the patients, due to the high mass concentration in contrast agents for CT. Thus, tantalum based solutions is the best overall option. With and image contrast improvement of 60% compared to iodine based contrast agent, at the highest x-ray tube potential.

Experiments and studies preformed by Nowak et al. [6] and Shilo et al. [7] explores methods of reducing administered dose to patients, by using high-Z solutions. They proceed with two different approaches. Nowak et al. [6] utilize the concept that high-Z solutions yield a higher contrast-to-noise ratio (CNR) at doses equal to those given by the commercial contrast agents. Thus, the administered dose can be decreased by using high-Z solutions to achieve the same CNR as the commercially used contrast agent. The experiments demonstrates that high-Z solutions performance varies with the x-ray tube potential and filter. Gadolinium based solution demonstrates a dose reduction of 19-60% for children and lean patients, hafnium based solution demonstrates a dose reduction 35-76% and 62-78% for average and obese patients respectively, and gold based solutions demonstrates a dose reduction of 74-86% for strongly obese patients. Shilo et al. [7] utilize the concept that nanoparticles (NPs) have a higher x-ray interaction cross section in the soft tissue. Thus, should be favored in the absorption of x-rays, and decrease the administered dose while increasing the image contrast. The studies demonstrate that gold, bismuth and tantalum NPs based solutions are of interests. Of these, gold NPs is especially interesting due to additional optical advantages, while bismuth and tantalum NPs are more economically favorable options.

2.1.2 Magnetic Resonance Imaging

In MRI it is the magnetic properties of the tissues that are utilized, which is presented in equation (3.2), found under chapter 3.1 Equations [14]. Thus, MRI does not utilize ionizing radiation, but is based on nuclear magnetic resonance (NMR). It is based on the concept that NMR can be used to detect unhealthy tissues [14], due to the different nuclear magnetic relaxation times of unhealthy and healthy tissues, which can generate a natural image contrast [14]. Though, in some cases the natural image contrast is not enough to differentiate between unhealthy and healthy tissues [14]. In those cases a contrast agent can be used to further enhance the imaging contrast in the area of interest [14].

The tissues in the human body is defined by the different relaxation times, T_1 and T_2 [14]. Thus, contrast agents can be classified as T_1 and T_2 contrast agents, with the purpose to reduce the T_1 and T_2 relaxation times of water protons [14, 15]. Since approximately 63% of the atoms in the human body is hydrogen atoms [14]. The purpose of T_1 agents is to reduce the longitudinal proton relaxation time, which is based on the transfer rate of excited energy from the proton to the surrounding medium [14]. While the purpose of T_2 agents is to reduce the transverse proton

relaxation time, which is based on the out of phase rate between protons [14].

Commercial T_1 agents are mainly gadolinium based, with the exception of one approved manganese based contrast agent [14, 15]. T_1 agents has a positive effect, causing an increase in the MRI signal, giving a bright signal [14, 15]. While T_2 agents are iron oxide nanoparticles (IONP) bases contrast agents [14, 15]. T_2 agents have a negative effect, causing a decrease in the MRI signal, giving a dark signal [14, 15]. Of these, iron based contrast agent is less toxic, while gadolinium based contrast agents are more toxic, due to its ability to replace the calcium ions present in the body [14, 15]. In addition to gadolinium not being stable for the pH of the body, thus it can form gadolinium hydroxide crystal deposits which can block vessels [14]. Currently gadolinium is administered as part of a complexes of chelates to overcome these problems [14]. However experiments investigating other options to mitigate the toxicity and stability issues has been conducted.

Experiments preformed by Zhang et al. [15] explores another method to toxicity and stability issues with gadolinium based contrast agents. By coating gadolinium with a layer of gold with the intent to provide air and water stability to gadolinium. Their experiments demonstrates a clear chemical stability of gadolinium coated with gold. However, the nanocrystals studied are not optimized and the relevance of some mechanisms are not obvious in regards to the chemical stability.

2.2 Space Exploration

Within the field of space exploration, high-Z materials are used in solid structural shielding, in order protect astronauts as well as electronics from the harmful ionizing and particle radiation present in space.

2.2.1 Shielding

With regards to radiation shielding of spacecrafts or habitats, there are two different building concepts [10]. An integrated concept where the most or all surfaces are covered by the shielding material, and it is a part of the structure, or a spot shielding concept, where only some parts of the surface is covered [10]. Also, there are two different shield compositions concepts: it can be a composite-Z shield composed of two layers of composite material with a layer with a high-Z material in between [9, 10]. Or it can be a graded-Z shield composed of a outer layer of high-Z material followed by layers of low-Z materials [8, 10].

High-Z materials are effective at stopping electrons and absorbing γ-rays, but less effective at stopping protons [8, 9, 10]. However low-Z materials are effective at stopping protons [8, 9, 10]. Thus it is of interest to construct multi layered shielding for space traveling of both low- and high-Z materials, i.e. composite-Z and graded-Z shielding. [9]. The commonly considered high-Z materials is gadolinium, tantalum and tungsten based materials, due to their different favorable characteristics [10]. Gadolinium has the larger neutron absorption cross section, and can be

utilized in situations were a large amount of secondary neutrons are present [10]. While tantalum and tungsten has better electron and photon attenuation, where of tungsten is slightly better but of the three has the lesser neutron absorption cross section [10]. Several experiments have been conducted to further investigating the two composition concepts and the different high-Z materials, for use both within the geosynchronous orbit (GSO) and beyond the high earth orbit (HEO), for future deep space traveling, as well as weight reduction of the shielding and improved radiation protection.

Experiments preformed by Atxaga et al. [9] and Klamm [9] explores shield composition concepts intended for use within GSO. Atxaga et al. [9] demonstrates that a composite-Z shield of tantalum or tungsten has a weight saving of 25%, compared to aluminium shield with the same radiation protection capacity for electron dominated environments. Klamm [10] explores the shielding properties of layers of a low-Z resin, high density polyethylene (HDPE) or polyphenolic, doped with microparticles of a high-Z material, tungsten, in layer configurations corresponding to both shield configurations, replacing the layers of pure low- and high-Z materials. The experiments demonstrates a composite-Z shield configuration preforms better over all then a graded-Z shield configuration. It also demonstrates that a phenolic resin is preferable in electron dominated environments, while HDPE in particle dominated environments.

Other experiments were preformed by Atwell et al. [8] while different graded-Z shielding configurations, under different space weather related conditions, GCR and SPEs. The experiments demonstrated that a graded-Z shielding of tantalum or tungsten with a inner layer of HDPE provided better radiation protection then a aluminium shield against GCR. While just a layer of HDPE provided better radiation protection then a graded-Z shield with high-Z materials against SPEs.

2.3 Elements of interest

Table (2.1) summarize the high-Z elements of interest utilized in the studied research material.

Table 2.1: High-Z elements of interest.

Element	Symbol	Z	Use	Reference
Iodine	I	53	CT	[5] [6] [7]
Barium	Ba	56	CT	[5]
Gadolinium	Gd	64	MRI, Space, Res.	[5] [6] [14] [10]
Holmium	Ho	67	Res.	[6]
Ytterbium	Yb	70	Res.	[5] [6]
Hafnium	Hf	72	Res.	[6]
Tantalum	Ta	73	Space, Res.	[5] [7] [8] [9] [10]
Tungsten	W	74	Space, Res.	[6] [8] [9] [10]
Osmium	Os	76	Res.	[6]
Gold	Au	79	Res.	[5] [6] [7] [15]
Bismuth	Bi	83	Res.	[5] [6] [7]

3
Theory

3.1 Equations

The intensity of the transmitted rays radiation (I) is given by (3.1):

$$I = I_0 e^{-\mu\chi} \tag{3.1}$$

where (I_0) is the intensity of the incident rays or radiation,(μ) is the attenuation coefficient of an absorbing medium and (χ) is its thickness [7].

The magnetization (M) of a medium is given by (3.2):

$$M = \chi H \tag{3.2}$$

where (χ) is the magnetic susceptibility of the medium, which is its ability to be magnetized by a magnetic field (H) [14].

The absorbed dose (D) is given by (3.3):

$$D = \frac{A}{\varepsilon l \rho G(Fe^{3+})} \tag{3.3}$$

where A is the change in absorbance, (ε) is the molar extinction coefficient, (l) is the cuvette path length , (ρ) is the density of the solution and ($G(Fe^{3+})$) is the yield of iron(III) [16].

The yield of iron(III) ($G(Fe^{3+})$) is given by (3.3):

$$G(Fe^{3+}) = 2G(H_2O_2) + 3[G(e^-_{aq}) + G(\bullet H) + G(\bullet HO_2)] + G(\bullet OH) \tag{3.4}$$

where $G(H_2O_2)$, $G(e^-_{aq})$, $G(\bullet H)$, $G(\bullet HO_2)$, and $G(\bullet OH)$ is given for acidic solution [16].

The activity (A) is given by (3.5):

$$A = A_0 e^{-\lambda t} \tag{3.5}$$

where A_0 is the activity at start time, λ is the decay constant of an isotope and t is the time passed [17].

3.2 Space radiation

Space radiation is unlike the radiation experienced on earth [18]. It is primarily made up of GCR, SPEs and the energetic protons and electrons in the Van Allen radiation belts surrounding the earth [18, 19]. Of these SPEs and GCR are of most concern for space exploration beyond LEO [19]. The large infrequent SPEs poses as radiation risk due to unpredictability, while steady low-dose GCR is a risk due to the lack of satisfactory shielding [3, 18, 19].

Space radiation is associated with the behaviour of the Sun and especially the solar activities , for example such as the 11 year solar cycle, the 27 days solar rotation and the sub-seconds eruptions [18, 20]. During the solar cycle there are periods of solar minimum and solar maximum, presented in figure (3.1), where the amount of sunspots are less during solar minimum then during solar maximum [3]. The intensity of GCR is higher during solar minimum, and lower during solar maximum [3, 18]. During solar maximum large ejections of plasma following eruptions on the sun surface is more frequent [3]. These are also known as Coronal Mass Ejections (CMEs) and are more frequent, which causes the SPEs [3].

Figure 3.1: Number of average sunspot per month [3].

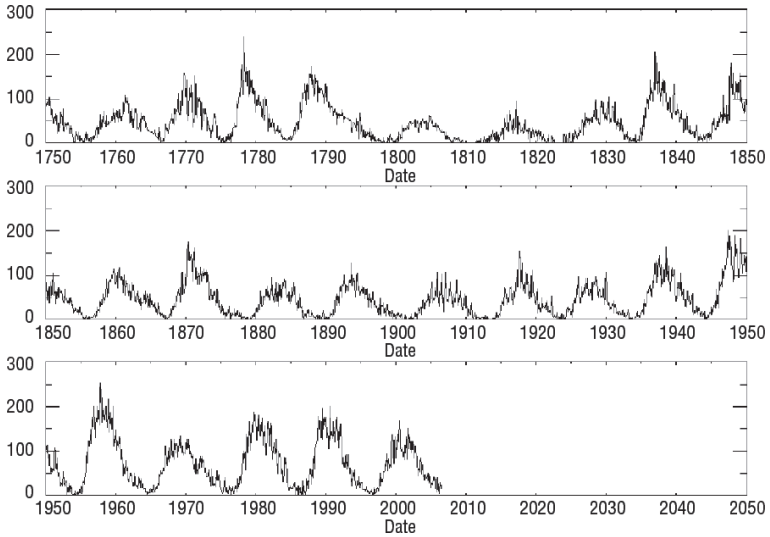

3.3 Dose

On a radiation protection basis, an astronaut is essentially considered the same as a radiation worker [21]. The radiation protection program for space travels follows the same as low as reasonably achievable (ALARA) principle as radiation protection programs for all work with ionizing radiation, e.g. Nuclear Chemistry at Chalmers University of Technology [21, 22]. In addition to the ALARA principle, dose assessment and management are prevailing factors when planing space missions, as well as

designing equipment and living quarters [21]. Figure (3.2) shows a simplified model for dose assessment scheme used for LEO [21].

However, despite the same approach to radiation protection for astronauts as for radiation workers, the yearly limit is not the same [3]. The limits set by NASA is at 500mSv for their astronauts in contrast to 20mSv for radiation workers in Sweden [3, 22]. However, the type for radiation is different, and space radiation is not equivalent to the radiation exposed on the Earth [3, 18]. 1mSv of space radiation can be approximated to receiving three chest x-rays on the Earth [3]. Furthermore, NASA operates with career exposure limits for their astronauts, presented in table (3.1) [3]. The limits are lower for young astronauts, due to the presumption that being exposed to large amounts of radiation at a young age can cause a higher health risks later in life [3]. These limits can be compared to radiation doses from previous missions, as well as predicted dose for a mission to Mash, presented in table (3.2) [3].

Figure 3.2: Simplified dose assessment to estimate received dose from LEO missions [21].

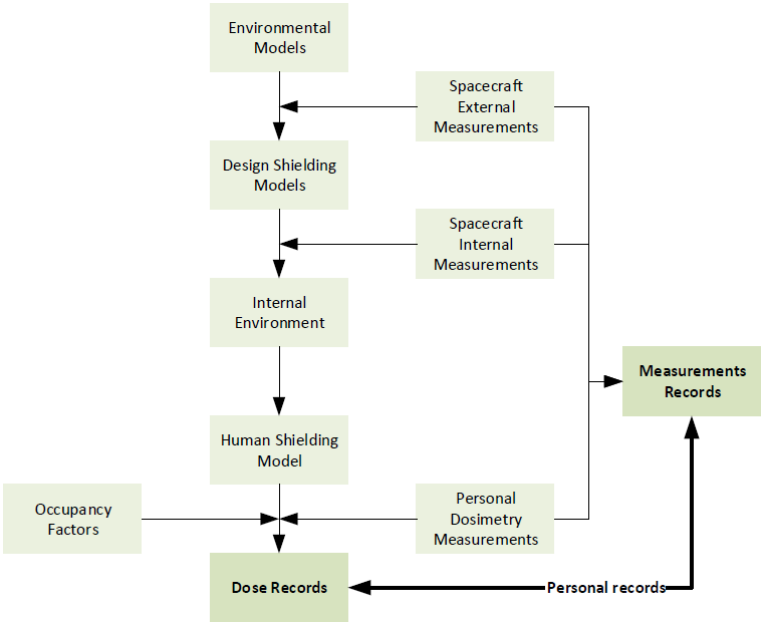

Table 3.1: Career exposure limits in mSv, by age and gender, by NASA [3].

Age	Male		Female	
	Radiation dose [mSv]	X-ray equivalent	Radiation dose [mSv]	X-ray equivalent
25	1500	4500	1000	3000
35	2500	7500	1750	5250
45	3250	9750	2500	7500
55	4000	12000	3000	9000

Table 3.2: Received and predicted radiation doses, by NASA [3].

Mission	Duration [days]	Radiation dose [mSv]	X-ray equivalent
Space Shuttle Mission 41-C	8	5.59	17
Apollo 14	9	11.4	35
Skylab 4	87	178	534
ISS Mission	183	160	480
Mars Mission	1096	1200	3600

3.4 Spacesuit

The spacesuits used by astronauts are divided into three categories. Intravehicular activity (IVA) suits, extravehicular activity (EVA) suits and the combined IEVA suits [23]. The space agencies are currently exclusively using separate IVA and EVA suits, though the first suits to be used for EVA was IEVA suits [23]. The spacesuits protects the astronauts during space exploration missions, especially during EVA [11, 23]. The suite shall protect against the space environment and its ionizing radiation, which of the latter is related to health risk concerns [11, 23].

3.4.1 Intravehicular activity suit

The IVA suit is also know as the rescue suit, and is worn during stays in space vehicles, i.e. during launch, travel and entry [23]. It is a lighter and thinner suit, design to accommodate conditions arising during launch and entry, e.g. vibrations, as well as providing a comfort to the astronaut [23]. Its purpose is to keep the astronauts safe in case of malfunctions or emergency situation in space vehicles [23]. Thus, it has basic survival systems, e.g. emergency oxygen tank, flotation systems, liquid cooling garments (LCG), parachute and several other features [23].

3.4.2 Extravehicular activity suit

The EVA suit enables astronaut to exit space vehicles and preform tasks in space [23]. It may differ slightly depending on the task intended to preform while in the suit, but is has some general requirements, e.g. to protect against radiation, temperatures, travelling particles, and several other features [23]. The suit consist of separate parts, of which the major ones are the upper torso which includes the the hard upper torso (HUT) and arm assembly, EVA gloves, lower torso assembly (LTA) and helmet, and also the primary life support subsystem (PLSS), communications carrier assembly (CCA) and the LCVG [11, 24].

3.4.3 Liquid cooling and ventilation garment

The space suites are designed to be insulating to protect the astronauts against the high and low temperatures occurring in the space environment [23]. The temperature inside the suit will stabilize around the astronauts body temperature, commonly 37^oC, because of the insulating abilities [23]. This is already a unfavorable temperature for activity [23]. In addition, as the astronaut is in activity more body heat is generated, and the temperature inside the suite increases [23]. The body will start sweating to cool of the body, and humidity will build-up within the suit, ultimately causing the astronaut to overheat or become dehydrated [23].

The LCG and LCVG is designed to regulate the temperature within the suit [23]. They are both skintight suits of nylon with a cotton mesh or of spandex, for LCG plastic tubes are weaved through the mesh, while for LCVG the plastic tubes are thread through sewed tracks [23, 24]. The astronauts body heat is then lead away by circulating water through the plastic tubes [23, 24]. With the LCVG the ventilation system is integrated in the skintight suits, primary made for ease for donning the EVA suit [23].

3.5 Dosimetry

Fricke dosimetry, is a measuring technique which can be used in the range 1-500 Gy [17]. The principle of the technique is to determine the iron(III) content formed by irradiation of a Fricke solution [17]. This is done by measuring the change in absorbance at 303nm spectrophotometrically, and using equation (3.3), found under chapter 3.1 Equations [17, 25]. The irradiation causes the oxidation from iron(II) in the Fricke solution to iron(III), according to the following reaction scheme [17].

$$e^-_{aq} + H^+ \rightarrow H\bullet$$
$$H\bullet + O_2 \rightarrow \bullet HO_2$$
$$\bullet HO_2 + Fe^{2+} \rightarrow Fe^{3+} + HO^-_2$$
$$HO^-_2 + H^+ \rightarrow H_2O_2$$
$$H_2O_2 + Fe^{2+} \rightarrow Fe^{3+} + OH^- + \bullet OH$$
$$\bullet OH + Fe^{2+} \rightarrow Fe^{3+} + OH^-$$

Ferrous-cupric dosimetry is a modification of Fricke dosimetry [16]. The solution contains copper in addition to iron, which extends the upper limit to the measurable dose range to approximately 5kGy [16]. This limit can be further extended by increasing the concentration of iron and copper [16].

4
Methods

The conditions for these experiments is that the water in the LCVG would be changed with the high-Z solutions. Thus, the high-z solutions should still function as a cooling liquid in addition to demonstrate shielding qualities. However, only the shielding properties are measured in these experiments. To mimic the water tubing in the LCVG a plastic tube was coiled up to fit around a 20ml glass vial, seen in figure (4.1), under chapter 4.2 High-Z solutions. A further detailed list of chemical and equipment can be found in appendix A.

4.1 Compounds

Table (2.1) was utilized to decide which high-Z elements to further investigate, and table (4.1) summarize the decision making process. The properties that was under consideration was if there were water solubility compounds, and the compounds health hazard rating by the European hazard symbols. This information was retrieved from American elements [26].

Firstly the elements currently used for structural shielding and research of said shielding was considered, e.i. gadolinium, tantalum and tungsten. Of these tantalum and tungsten was discarded due to their health hazard ratings, while gadolinium was selected in the form of gadolinium(III) chloride, $GdCl_3$. Thereafter, gold, ytterbium and bismuth was considered due to their use in several of the reference material. Of these gold was discharged to it being a expensive option and bismuth due to few water soluble options, while ytterbium was selected in the form of ytterbium(III) chloride, $YbCl_3$. Lastly barium was considered due to the current use in CT, but disregarded due to few water soluble options. Thus, cerium was considered and selected in the form of cerium(III) chloride, $CeCl_3$. To have one element between each decimal range, Z=50-59, 60-69. 70-79, for a wide range of elements. Lead was chosen to use as a sort of reference, in the form of lead(II) nitrate. Since this is a reoccurring element used in structural shielding in laboratories, thus the health hazard rating is disregarded in this case.

Table 4.1: Element decision, summary [26]

Element	Symbol	Z	Selected	Note
Barium	Ba	56	×	Few water soluble options
Cerium	Ce	58	$CeCl_3$	
Gadolinium	Gd	64	$GdCl_3$	
Ytterbium	Yb	70	$YbCl_3$	
Tantalum	Ta	73	×	Health hazard rating
Tungsten	W	74	×	Health hazard rating
Gold	Au	79	×	Expensive
Lead	Pb	82	$Pb(NO_3)_2$	
Bismuth	Bi	83	×	Few water soluble options

4.2 High-Z solutions

The high-Z solutions were prepared by dissolving the previously mentioned compounds in Milli-Q water. 25ml solution was prepared for the experiments using a self made plastic coil. While for he experiments using a jacketed beaker, 50ml solution was prepared. The salts were measured up according to table (4.2) and (4.3) and added to separate 50ml plastic vials. The vials were filled up to 25ml or 50ml with Milli-Q water, and then shaken until the salt was fully dissolved.

The self made plastic coil, seen in figure (4.1), was filled with 20ml high-Z solution using a plastic syringe, from the prepared 25ml high-Z solution. The syringe was used to ensure no air bubbles in the coil also some of the solution is flushed through the coil to wash out possible residuals. To clog the coil, cut offs from 1ml plastic bulb pipettes was pushed into each end. At the bottom end, Lubriseal Stopckock Grease was used to ensure no leakage, and for the top end two holes in the plastic bulb pipette ensure no over pressure in the coil.

Figure 4.1: Photo of the self made plastic coil.

The outer chamber of the jacketed beaker, seen in figure (4.2), was filled with 40ml high-Z solution using a plastic syringe, from the prepared 50ml high-Z solution. The syringe was used due to more convenient handling when filling the outer chamber. To clog the jacketed beaker a plastic cap and Parafilm was used. At the bottom end, the plastic cap was pressed into places, Parafilm is wrapped around it to ensure no leakage, and for the top end Parafilm was used to cover the hole allowing expansion due to possible over pressure. Also a plastic lid was loosely placed over the inner chamber of the jacketed beaker.

Figure 4.2: Photo of the jacketed beaker.

After use the self made plastic coil and syringe was rinsed with Milli-Q water twice. While the jacketed beaker was rinsed like regular laboratory glassware, with a final rinse of Milli-Q water.

Table 4.2: 25ml high-Z solution.

Element	Symbol	Z	Salt	Conc. element [g/l]	Amount for 0.025l [g]
Cerium	Ce	58	$CeCl_3 \bullet 7H_2O$	10	0.6648
Gadolinium	Gd	64	$GdCl_3 \bullet 6H_2O$	10	0 5909
Ytterbium	Yb	70	$YbCl_3 \bullet 6H_2O$	10	0.5598
Lead	Pb	82	$Pb(NO_3)_2$	10	0.3996
Cerium	Ce	58	$CeCl_3 \bullet 7H_2O$	20	1.3296
Gadolinium	Gd	64	$GdCl_3 \bullet 6H_2O$	20	1.1818
Ytterbium	Yb	70	$YbCl_3 \bullet 6H_2O$	20	1.1196
Lead	Pb	82	$Pb(NO_3)_2$	20	0.7992
Lead	Pb	82	$Pb(NO_3)_2$	30	1.1988
Lead	Pb	82	$Pb(NO_3)_2$	300	11.9884

Table 4.3: 50ml high-Z solution.

Element	Symbol	Z	Salt	Conc. element [g/l]	Amount for 0.050l [g]
Lead	Pb	82	$Pb(NO_3)_2$	300	23.9768

4.3 Dosimetry

A fresh batch of the dosimetry solutions were made for each measurement. The Ferrous-cupric solutions was always made in batches of 100ml and only used with the self made plastic coil. While the Fricke solution was made in batches of 50ml used with the jacketed beaker, and 100ml used with the self made plastic coil.

Five 20ml glass vials was filled with 15ml dosimetry solution for all the experiments preformed with the self made plastic coil . While for other experiments only using glass vial, a various number of glass vials was filled with 10ml dosimetry solution. The inner chamber was filled with 15ml dosimetry solution for the all the experiments preformed with the jacketed beaker, and also one 20ml glass vial filled with 15ml dosimetry solution. Between the experiments the glass vials were washed like regular laboratory glassware and dried over night, for reuse.

4.3.1 Ferrous-cupric solution

Iron(II) sulfate- and copper(II) sulfate salts were measured up according to table (4.4), and added to a 100ml volumetric flask. Thereafter, the volumetric flask was filled up to 100ml with 0,005M sulfuric acid. The flask was shaken until the slats were fully dissolved.

Table 4.4: 100ml Ferrous-cupric solution.

Salt	Molar mass [g/mol]	Concentration [g/l]	Amount for 0.1l [g]
$FeSO_4 \bullet 7H_2O$	278.02	0.001	0.0278
$CuSO_4 \bullet 5H_2O$	249.69	0.010	0.2497

4.3.2 Fricke solution

Ammonium iron(II) sulfate- and sodium chloride salts were measure up according to table (4.5) and (4.6), and added to a 50ml or 100ml volumetric flask. Thereafter, the volumetric flask was filled up to 50ml or 100ml with 0,4M sulfuric acid. The flask was shaken until the salts were fully dissolved.

Table 4.5: 50ml Fricke solution.

Salt	Molar mass [g/mol]	Concentration [mol/l]	Amount for 0.1l [g]
$Fe(NH_4)_2(SO_4)_2 \bullet 6H_2O$	392.14	0.001	0.0196
$NaCl$	58.44	0.001	0.0029

Table 4.6: 100ml Fricke solution.

Salt	Molar mass [g/mol]	Concentration [mol/l]	Amount for 0.1l [g]
$Fe(NH_4)_2(SO_4)_2 \bullet 6H_2O$	392.14	0.001	0.0392
$NaCl$	58.44	0.001	0.0058

4.4 Irradiation

The irradiation of the samples were preformed in a Gammacell 220 loaded with a Co^{60} source, a 900TBq source loaded in 2010. Several different experimental configurations were used, and they are illustrated in figure (4.3-4.7). These illustrations are not to scale. The reoccurring larger lighter gray circle illustrates the irradiation chamber, and the smaller darkest gray circle illustrates the glass vials. The lids were left slightly open to ensure no over pressure in the glass vials.

Figure (4.3) was the configuration used for estimating the dose using Ferrous-cupric dosimetry, for this configuration one sample was periodically removed with one minute interval. Effectively meaning that one sample was irradiated for one minute, one for two minutes, one for three minutes, one for four minutes, and one for five minutes.

Figure 4.3: Ferrous-cupric dosimetry, dose estimation, configuration of samples in Gammacell 220.

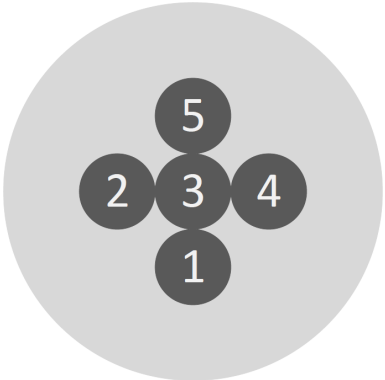

Figure (4.4) was the configuration used for estimating the dose using Fricke dosimetry, for this configuration the samples was placed into the gammacell three one by one. These samples was irradiated for even time intervals within five minutes. Effectively meaning that one sample was irradiated for one minute and 40 seconds, one for three minutes and 20 seconds, and one for five minutes.

Figure 4.4: Fricke dosimetry, dose estimation,configuration of sample in Gammacell 220.

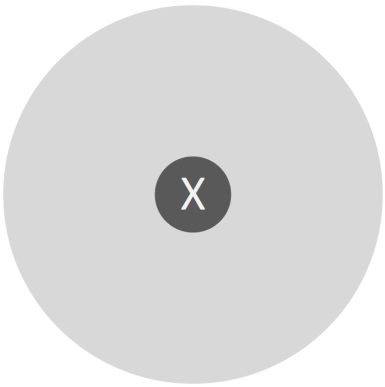

Figure (4.5) was the configuration used with the self made plastic coil. The yellow figure illustrates the self made plastic coil, for this configuration the four samples was placed into the gammacell one by one, within the plastic coil. These samples was irradiated for even time intervals within five minutes. Effectively meaning that one sample was irradiated for one minute and 15 seconds, one for two minuets and 30 seconds, one for three minutes and 45 seconds, and one for five minutes.

Figure 4.5: Self made plastic coil configuration of sample in Gammacell 220.

Figure (4.6) was the configuration used with the jacketed beaker. The blue figure illustrates the jacketed beaker, for this configuration the jacketed beaker was irradiated for two samples. These samples was irradiated for even time intervals within five minutes. Effectively meaning that one sample was irradiated for two minutes and 20 seconds, and one for five minutes. Between the two samples the dosimetry solutions was changed and the inner chamber washed.

Figure 4.6: Jacketed beaker configuration of sample in Gammacell 220.

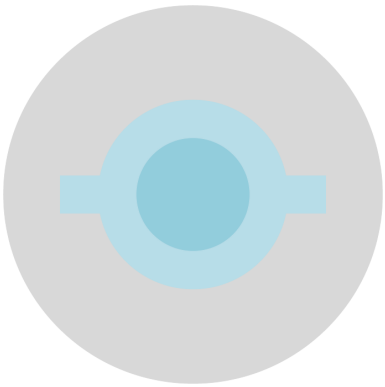

Figure (4.7) was the configuration used with solid lead. The darker figure illustrates the solid lead shield, for this configuration the three samples was placed into to the gammacell one by one, within the solid lead shield. These samples was irradiated for even time intervals within five minutes. Effectively meaning that one sample was irradiated for one minute and 40 seconds, one for three minutes and 20 seconds, and one for five minutes.

Figure 4.7: Solid lead shield configuration of sample in Gammacell 220.

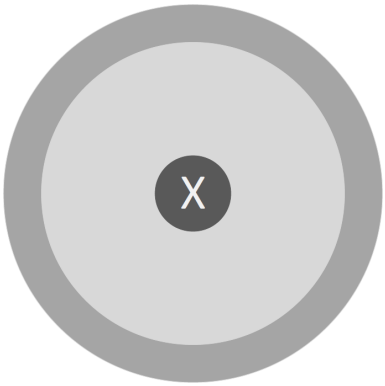

4.5 UV/VIS spectrometer

After the irradiation, a Lambda 25 UV/VIS spectrometer was used to measure the absorption in the samples. The samples was shaken or stirred. A suitable amount of sample were taken form the lower half of the sample, and transferred into a 10mm square quarts cuvette. A suitable amount, means that the cuvette need to contain enough solutions to cover the measuring window of the machine. Prior to placing the filled cuvettes in the machine for measurements, the outer surface was wiped off with a sheet of Kleenex, to ensure no interference from dirt to the spectrum. The quarts cuvettes were rinsed with ethanol between each measurement for reuse.

5
Results

All the results are presented as linear fit function (y), estimated form a scatter plot of the experimental data. Included is also the linear fit coefficient (R^2), to indicate how close the function fit the experimental data presented.

In all graphs the measured dose in the Gammacell 220, is presented by a black line. In the experiment using the Ferrous-Cupric solution the dose was measured to be higher then the in experiments using the Fricke solution. This will be discussed further in chapter 6 Conclusion.

All the results from the self made plastic coil experiments are related to the dose measured when filled with Milli-Q water, since this mimics the current LCVG. While the results from the jacketed beaker are related to the dose in the Gammacell 220.

The graphs display the lower values obtained from the measurements, to relate to the previously mentioned yearly limit for astronauts. As a reminder the yearly limit for astronauts is 500mSv, which relates to 0.5Gy. However, the received and predicted dose for several space mission are significant lower then this.

5.1 Ferrous-Cupric Dosimetry

5.1.1 Self Made Plastic Coil

Figure (5.1) and table (5.1) present the results for a solution containing cerium. It appears to have some shielding qualities. The solution with 10g/l high-Z element demonstrate more shielding then Milli-Q water, the dose is decreased. While the solution with 20g/l demonstrates less shielding then Milli-Q water, the dose is increased.

Figure 5.1: Cerium shield solution.

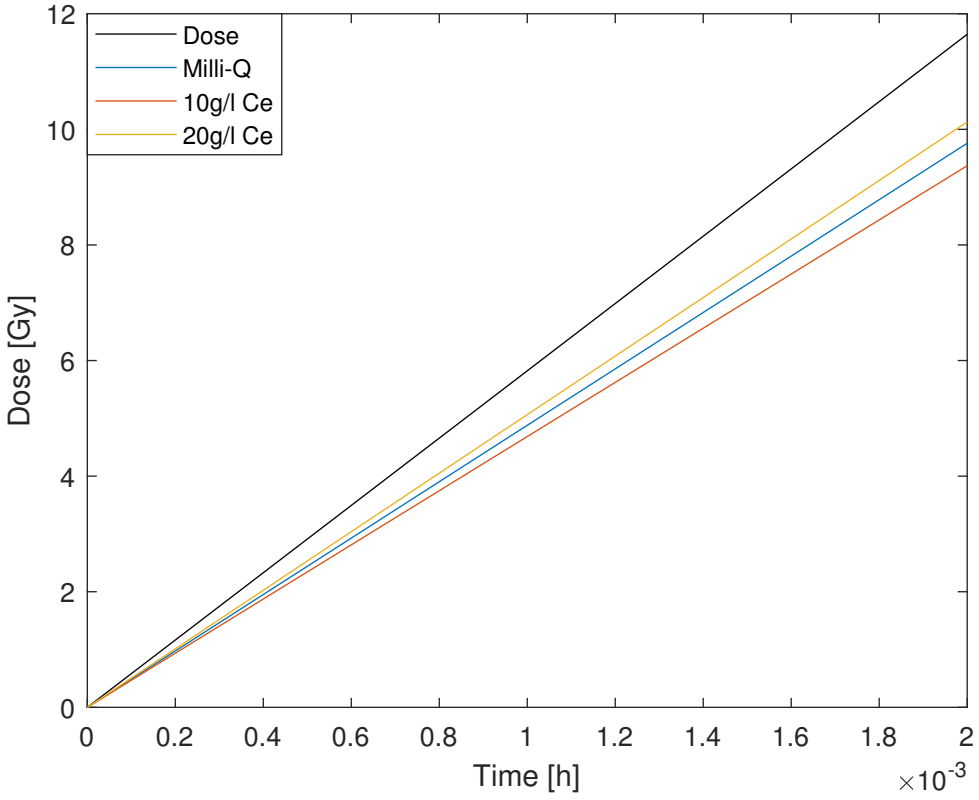

Table 5.1: Additional information to figure (5.1)

Colour	Name	Linear fit (y)	Linear fit (R^2)
Black	Dose	$5822.2 \times x$	0.9924
Blue	Milli-Q	$4879.7 \times x$	0.9979
Red	10g/l Ce	$4685.4 \times x$	0.9965
Yellow	20g/l Ce	$5064.8 \times x$	0.9973

Figure (5.2) and table (5.2) present the results for a solution containing gadolinium. Similar to the result for a solution containing cerium, it appears to have some shielding qualities. Again, the solution with 10g/l high-Z element demonstrates more shielding then Milli-Q water, the dose is decreased, though with a smaller margin. While the solution with 20g/l demonstrates less shielding then Milli-Q water, the dose is increased, also with a smaller margin.

Figure 5.2: Gadolinium shield solution.

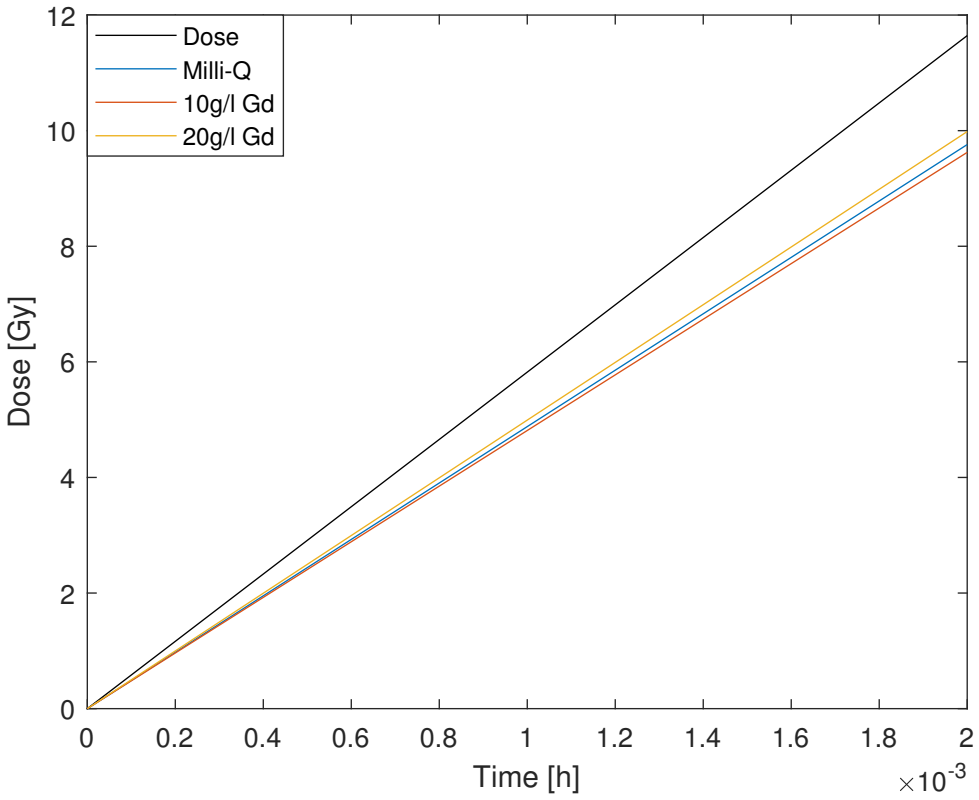

Table 5.2: Additional information to figure (5.2)

Colour	Name	Linear fit (y)	Linear fit (R^2)
Black	Dose	$5822.2 \times x$	0.9924
Blue	Milli-Q	$4879.7 \times x$	0.9979
Red	10g/l Gd	$4812.2 \times x$	0.9993
Yellow	20g/l Gd	$4992.1 \times x$	0.9997

Figure (5.3) and table (5.3) present the results for a solution containing ytterbium. Unlike the results for solution containing cerium and gadolinium, it appears to have no shielding qualities. Both the solution with 10g/l and 20g/l high-Z element demonstrate less shielding then Milli-Q water, the dose is increased.

Figure 5.3: Ytterbium shield solution.

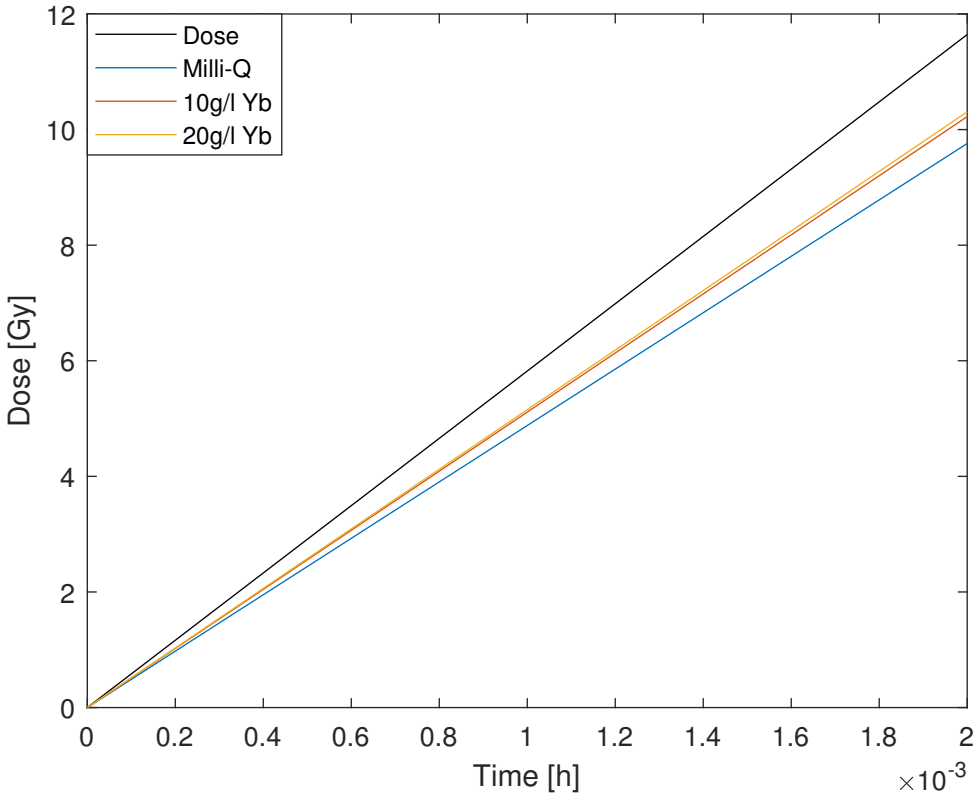

Table 5.3: Additional information to figure (5.3)

Colour	Name	Linear fit (y)	Linear fit (R^2)
Black	Dose	$5822.2 \times x$	0.9924
Blue	Milli-Q	$4879.7 \times x$	0.9979
Red	10g/l Yb	$5112.0 \times x$	0.9988
Yellow	20g/l Yb	$5153.7 \times x$	0.9963

Figure (5.4) and table (5.4) present the results for a solution containing lead. Similar to the results for solutions containing cerium, gadolinium and ytterbium, it appears to have some shielding qualities. However, the solution with 10g/l high-Z element demonstrates less shielding then Milli-Q water, the dose is increased. With a smaller margin, then the solution with 20g/l high-Z element demonstrates more shielding then Milli-Q water, the dose is decreased.

Figure 5.4: Lead shield solution.

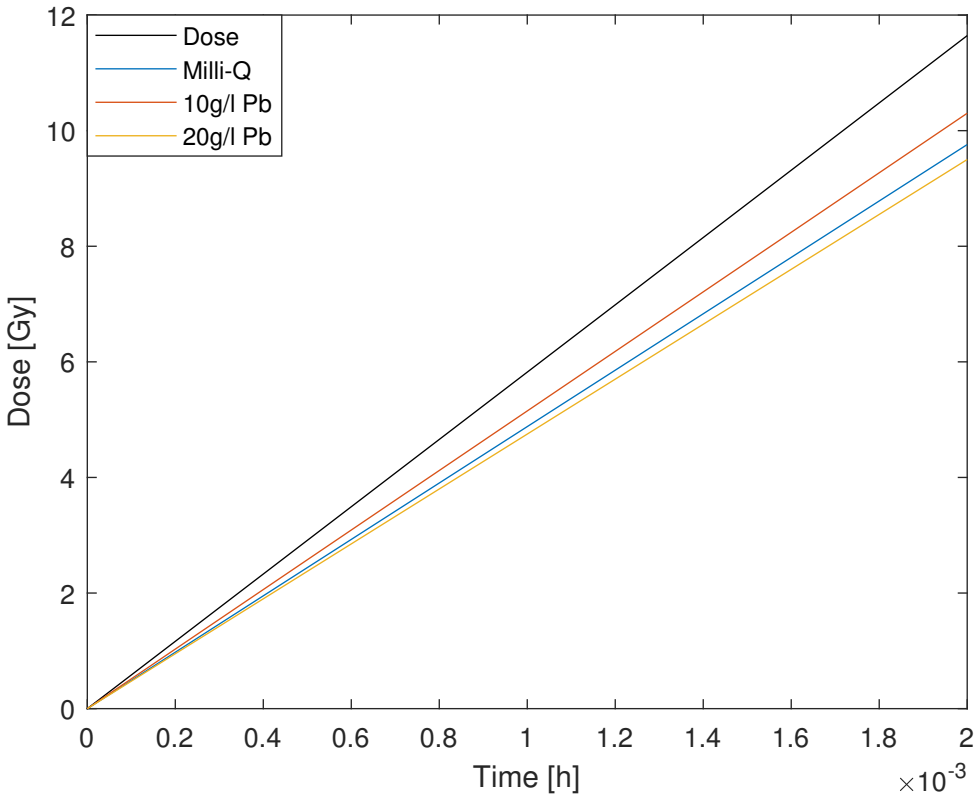

Table 5.4: Additional information to figure (5.4)

Colour	Name	Linear fit (y)	Linear fit (R^2)
Black	Dose	$5822.2 \times x$	0.9924
Blue	Milli-Q	$4879.7 \times x$	0.9979
Red	10g/l Pb	$5150.7 \times x$	0.9964
Yellow	20g/l Pb	$4750.4 \times x$	0.9982

5.2 Fricke Dosimetry

5.2.1 Self Made Plastic Coil

Figure (5.5) and table (5.5) present the results for a solution containing lead. It appears no shielding qualities. The solution with 10g/l, 20g/l, 30g/l and 300g/l high-Z element demonstrates less shielding then Milli-Q water.

Figure 5.5: Lead shield solution.

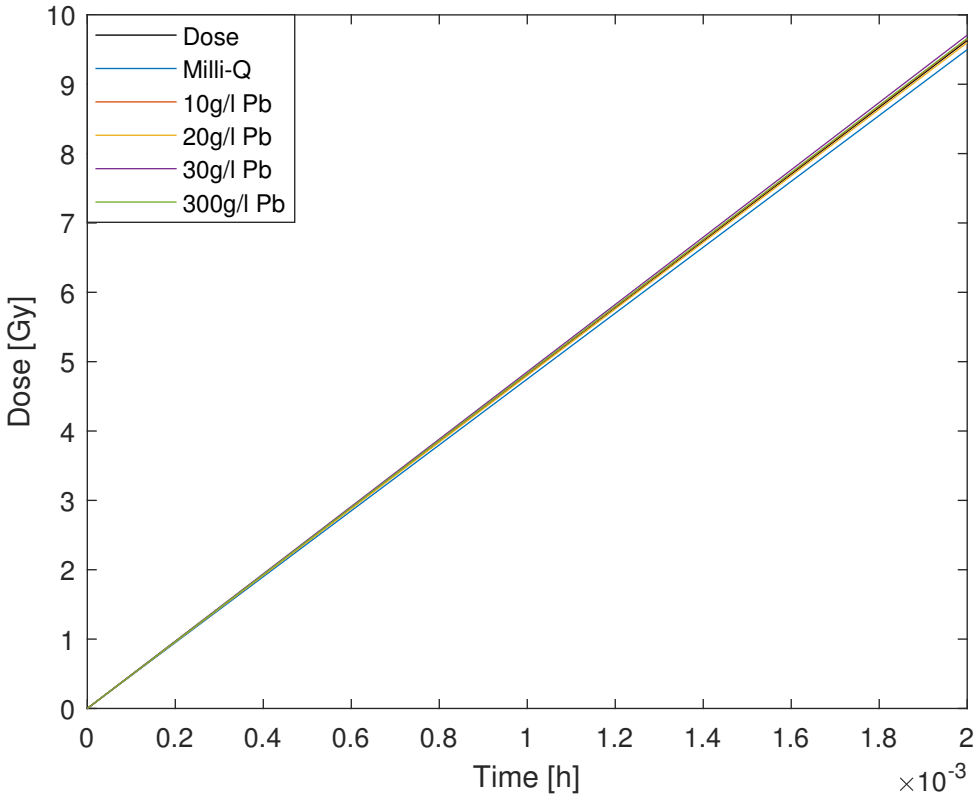

Table 5.5: Additional information to figure (5.5)

Colour	Name	Linear fit (y)	Linear fit (R^2)
Black	Dose	$4815.4 \times x$	0.9995
Blue	Milli-Q	$4749.6 \times x$	0.9992
Red	10g/l Pb	$4824.8 \times x$	0.9993
Yellow	20g/l Pb	$4799.5 \times x$	0.9995
Purple	30g/l Pb	$4853.6 \times x$	0.9996
Green	300g/l Pb	$4830.3 \times x$	0.9995

5.2.2 Jacketed Beaker

Figure (5.6) and table (5.6) present the results for a solution containing lead. It appears to have shielding qualities. The solution with 300g/l high-Z element in a approximately 0.5cm wide space demonstrates more shielding then Milli-Q water, the dose is decreased. While Milli-Q water demonstrates only slightly more shielding the dose in the Gammacell 220, the dose is decreased. Furthermore, in this experimental set up, the solution with 300g/l high-Z element demonstrates the most shielding compared to all the other results.

Figure 5.6: Lead shield solution.

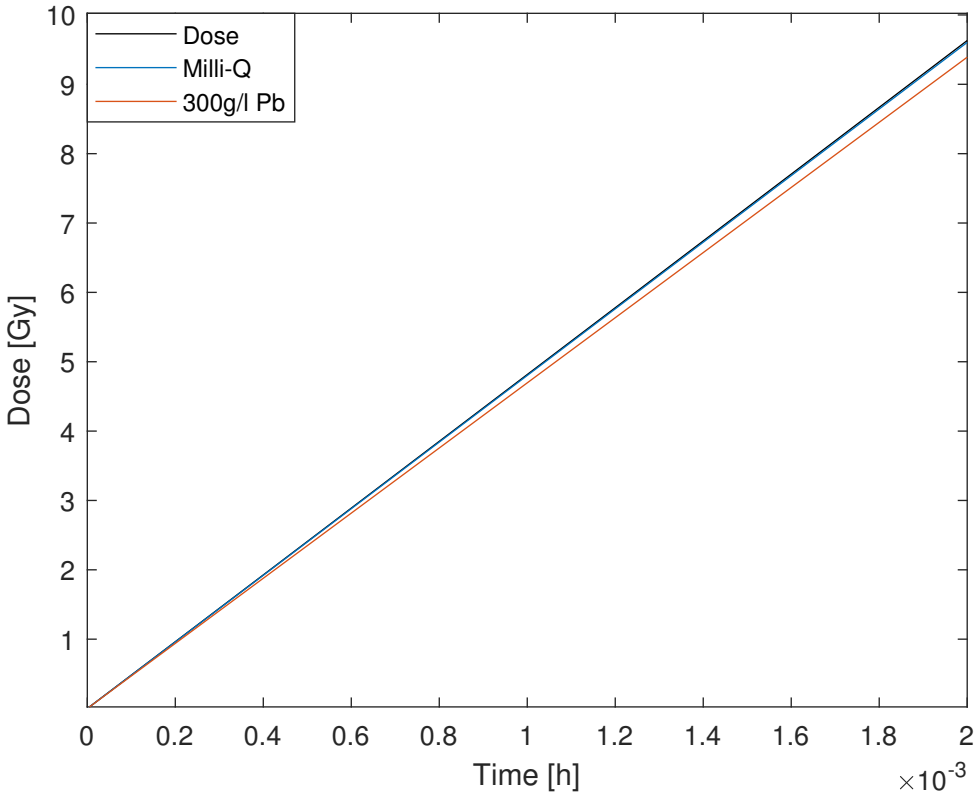

Table 5.6: Additional information to figure (5.6)

Colour	Name	Linear fit (y)	Linear fit (R^2)
Black	Dose	$4815.4 \times x$	0.9995
Blue	Milli-Q	$4802.1 \times x$	0.9998
Red	300g/l Pb	$4695.6 \times x$	0.9989

5.2.3 Solid Lead

Figure (5.7 and table (5.7) present the results for a 1.5cm solid lead shield. As expected, the solid lead shield demonstrate shielding. With a significantly larger margin then any of the high-Z solution.

Figure 5.7: Solid lead shield.

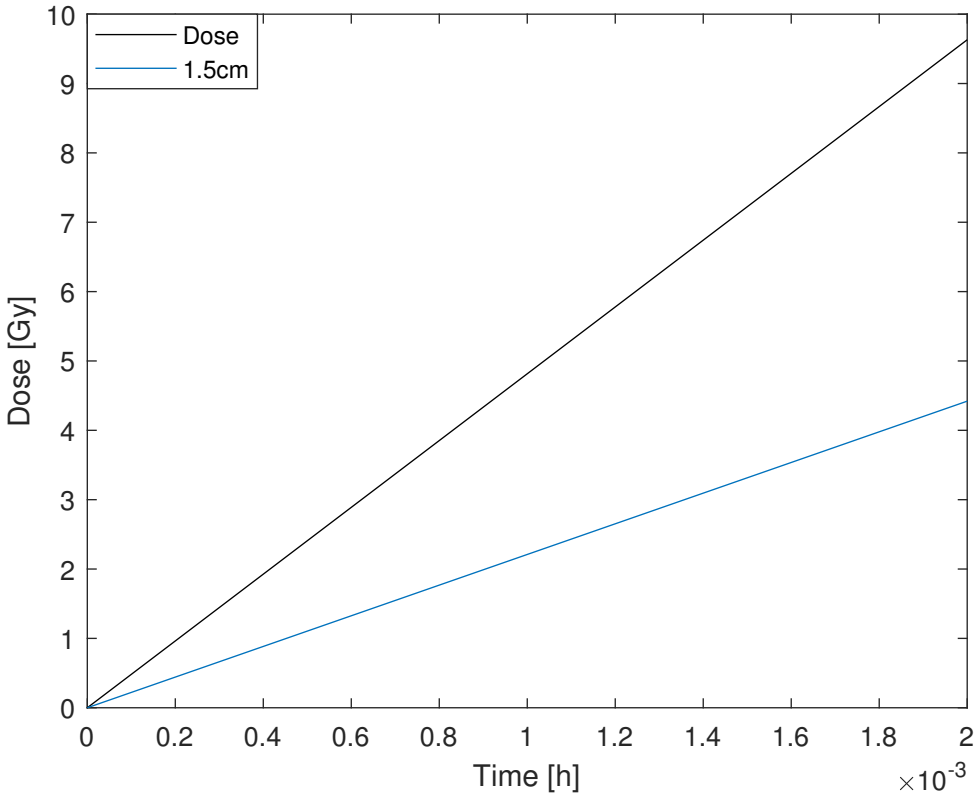

Table 5.7: Additional information to figure (5.7)

Colour	Name	Linear fit (y)	Linear fit (R^2)
Black	Dose	$4815.4 \times x$	0.9995
Blue	1.5cm	$2110.2 \times x$	0.9997

Figure (5.8) and table (5.8) presents estimated calculations using equation (3.1) for a 0.5cm, 1.0cm and 1.5cm solid lead shield. Similar to the results for a 1.5cm solid lead shield, the estimated calculations demonstrate shielding. Furthermore, that 0.5cm solid lead also demonstrate a shielding with significantly larger margin then any of the high-Z elements.

Figure 5.8: Solid lead shield.

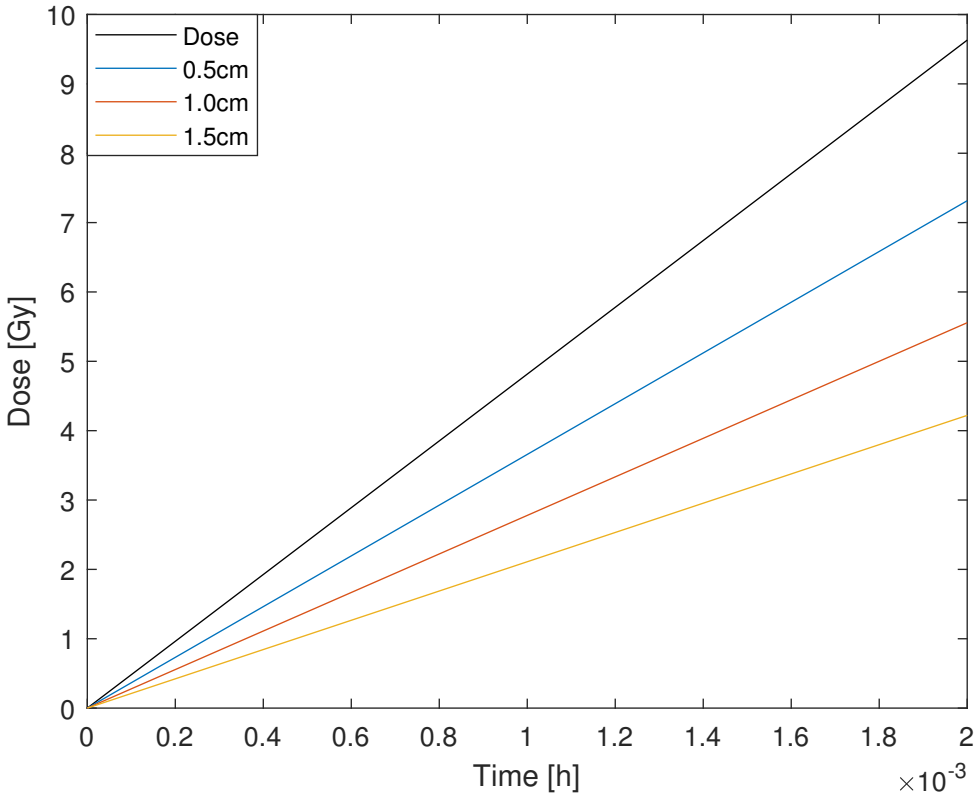

Table 5.8: Additional information to figure (5.8)

Colour	Name	Linear fit (y)	Linear fit (R^2)
Black	Dose	$4815.4 \times x$	0.9995
Blue	0.5cm	$3657.6 \times x$	0.9996
Red	1.0cm	$2778.2 \times x$	0.9996
Yellow	1.5cm	$2110.2 \times x$	0.9997

6
Conclusion

It should be pointed out that cerium(III)- gadolinium(III)- and ytterbium (III) chloride are all categorized as irritants according to the European hazard system [26]. Thus, it can be argued that non of them is a viable option to use in space exploration to begin with. Because astronauts most likely would require treatments if coming in contact with these solutions. However, they have been examined as potential contrast agents, which would ultimately be introduced to the human body. Thus, the experiments were conducted to establish the shielding potential.

Regarding the measured dose in the Gammacell 220, the dose measured with Ferrous-Cupric dosimetry is approximately 1kGy/h higher then measured Fricke dosimetry, as briefly mentioned previously. This could possibly be due to the different experimental setup used, for the dose measured with the Ferrous-cupric dosimetry all the samples was in the Gammacell 220 at the same time. Resulting in the vials having slightly different positions within the irradiation chamber. Appendix B contains measurements preformed by Ivan Kajan in connection with his PhD thesis, were it can be observed that the sample position within the irradiation chamber affects the measured dose. This can explain the discrepancy between the dose measured with Ferrous-Cupric dosimetry and Fricke dosimetry. Thus, the dose measured with Fricke dosimetry is believed to be the correct dose, due to this experimental set up being closer to the other experimental set ups, with one sample at the time in the middle of the irradiation chamber. Also, the dose measured with Fricke dosimetry correspond with the estimated present-day dose from previously preformed dose measurements, also based on Ivan Kajans measurements, found under Appendix B. Further backing this up as the correct measurement for present-day dose.

In regard to the experiments using Ferrous-Cupric dosimetry and the self made plastic coil. The results for 10g/l and 20g/l elemental concentration of shielding solution are not clear, there is no defined trend in dose reduction. The different high-Z elements and concentrations increase or decrease the dose in comparison to Milli-Q water. Compared to the yearly limit for astronauts this margin is approximately $<$40mSv which is a good margin in the case of decrease. However, compared to the received and predicted doses for space missions, which are significantly lower, this margin is proportionally lower. Thus, the decrease is much lower and less noticeable or significant.

The reason for first using Ferrous-Cupric dosimetry was based on recommendations due to previous conducted experiment for the Gammacell 220. However, from these experiments the estimated linear fit is closer to the data points with Fricke

dosimetry. Thus, it can be reasoned that for absorbed doses lower then the 500Gy limit using Ferrous-cupric dosimetry is less accurate than Fricke dosimetry. Since Fricke provides a better linearity. Thus, further focus is on the results from Fricke dosimetry.

In regard to the experiments using Fricke dosimetry, these experiments were only done for lead due to the availability of lead(II) nitrate. The results for the self made plastic coil are similar to the results from the Ferrous-Cupric dosimetry but with a smaller margin. Also for 30g/l and 300g/l elemental concentration of shielding solution. Compared to the yearly limit for astronauts this margin is approximately <10mSv, which is significantly smaller then the results from Ferrous-Cupric dosimetry. Also, for the jacketed beaker experiments was only done for a 300g/l elemental concentration of shielding solution. Compared to the yearly limit for astronauts decreases the dose with approximately <20mSv., which again will be proportionally lower for the received and predicted doses for space missions.

The final conclusion is based on the results from Fricke dosimetry. The self made plastic coil experiments, simulating the tubing in a LCVG, utilizing a lead shielding solution do not provide a significant dose reduction compared to previously mentioned received and predicted doses for space missions. Thus, it is not relevant to change out the water in the current design of LCVG to a high-Z solution. However, the jacketed beaker experiments, a larger surface covered with a lead shielding solution do provide a slight dose reduction. Thus, it can be relevant to consider this for future alternative designs of the LCVG, or for future habitat designs.

Although these experiments have not demonstrated the most desired outcome, there is still some possibilities to explore further. This would be to expand on the experiments using the jacketed beaker, with the larger surfaces covered with high-Z solution. Suggestions would be to run experiments with wider space for the shielding solution, so the layer of shielding solution is thicker. Another suggestion is to run experiments using other high-Z salts with a higher solubility constant, enabling the possibility for a higher elemental concentration then 300g/l. These suggestions were not explored due to time, and resources.

Bibliography

[1] NASA/JPL-Caltech/ESA/CXC/STScI. (2009, November 10). PIA12348 [Great Observatories Unique Views of the Milky Way]. Retrieved February 28, 2019, from https://images.nasa.gov/details-PIA12348.html

[2] Dunbar, B. (2015, March 16). Apollo 17. Retrieved from https://www.nasa.gov/mission_pages/apollo/missions/apollo17.html

[3] Rask, J., Vercoutere, W., Navarro, B. J., & Krause, A. (2007). *Space Faring The Radiation Challenge*. Huntsville, AL: National Aeronautics and Space Administration.

[4] Dunbar, B. (2015, January 26). What's Next For NASA? Retrieved from https://www.nasa.gov/about/whats_next.html

[5] FitzGerald, P. F., Colborn, R. E., Edic, P. M., Lambert, J. W., Torres, A. S., Bonitatibus, P. J., & Yeh, B. M. (2016). CT Image Contrast of High-Z Elements: Phantom Imaging Studies and Clinical Implications. *Radiology*, 278(3), 723-733. doi:10.1148/radiol.2015150577

[6] Nowak, T., Hupfer, M., Brauweiler, R., Eisa, F., & Kalender, W. A. (2011). Potential of high-Z contrast agents in clinical contrast-enhanced computed tomography. *Medical Physics*, 38(12), 6469-6482. doi:10.1118/1.3658738

[7] Shilo, M., Reuveni, T., Motiei, M., & Popovtzer, R. (2012). Nanoparticles as computed tomography contrast agents: Current status and future perspectives. *Nanomedicine*, 7(2), 257-269. doi:10.2217/nnm.11.190

[8] Atwell, W., Rojdev, K., Aghara, S., & Sriprisan, S. (2013). Mitigating the Effects of the Space Radiation Environment: A Novel Approach of Using Graded-Z Materials. *AIAA SPACE 2013 Conference and Exposition*. doi:10.2514/6.2013-5385

[9] Atxaga, G., Marcos, J., Jurado, M., Carapelle, A., & Orava, R. (2012). Radiation shielding of composite space enclosures. *International Astronautical Congress 2012*.

[10] Klamm, B. (2015). Passive Space Radiation Shielding: Mass and Volume Optimization of Tungsten-Doped PolyPhenolic and Polyethylene Resins. *Annual AIAA/USU Conference on Small Satellites 2015*

[11] Wilson, J. W., Anderson, B. M., Cucinotta, F. A., Ware, J., & Zeitlin, C. J. (2006). Spacesuit Radiation Shield Design Methods. *SAE Technical Paper Series*. doi:10.4271/2006-01-2110

[12] Izenson, M., Chen, W., Phillips, S., Chepko, A., Bue, G., Ferl, J., & Cencer, D. (2015). Multifunctional Cooling Garment for Space Suit Environmental Control. *International Conference on Environmental Systems 2015*

[13] Baiocco, G., Giraudo, M., Bocchini, L., Barbieri, S., Locantore, I., Brussolo, E., . . . Ottolenghi, A. (2018). A water-filled garment to protect astronauts during interplanetary missions tested on board the ISS. *Life Sciences in Space Research*, 18, 1-11. doi:10.1016/j.lssr.2018.04.002

[14] Laurent, S., Henoumont, C., Stanicki, D., Boutry, S., Lipani, E., Belaid, S., . . . Elst, L. (2017). *MRI contrast agents: From molecules to particles*. Singapore: Springer.

[15] Zhang, M., & Wagner, M. J. (2018). Gadolinum-gold core-shell nanocrystals: Potential contrast agents for molecular MRI with high T 1 relaxivity. *Journal of Magnetism and Magnetic Materials*, 454, 254-257. doi:10.1016/j.jmmm.2018.01.082

[16] Klassen, N. V., Shortt, K. R., Seuntjens, J., & Ross, C. K. (1999). Fricke dosimetry: The difference between $G(Fe^3)$ for ^{60}Co gamma-rays and high-energy x-rays. *Physics in Medicine and Biology*, 44(7), 1609-1624. doi:10.1088/0031-9155/44/7/303

[17] Choppin, G., Liljenzin, J., Rydberg, J., & Ekberg, C. (2014). *Radiochemistry and Nuclear Chemistry*. Amsterdam: Elsevier.

[18] *Understanding space radiation*. (2002). Houston, TX: National Aeronautics and Space Administration.

[19] *Information needed to make radiation protection recommendations for space missions beyond low-earth orbit* (NCPR report; no. 153). (2006). Bethesda, MD: National Council on Radiation Protection and Measurements.

[20] Lilensten, J. (2007). *Space Weather: Research Towards Applications in Europe*. Dordrecht: Springer.

[21] *Operational radiation safety program for astronauts in low-earth orbit: A basic framework ; commendations of the National Council on Radiation Protection and Measurements* (NCRP report; no. 142). (2002). Bethesda, MD: National Council on Radiation Protection and Measurements.

[22] Skarnemark, G., & Allard, S. (2019). *RADIATION PROTECTION*. Gothenburg: Chalmers University of Technology, Department of Chemistry and Chemical, Engineering, Nuclear Chemistry.

[23] Thomas, K. S., & McMann, H. J. (2012). *U.S. Spacesuits* (2nd ed.). New York, NY: Springer New York.

[24] Dunbar, B. (2013, June 05). Learn About Spacesuits. Retrieved February 22, 2019, from https://www.nasa.gov/audience/foreducators/spacesuits/home/clickable_suit_nf.html

[25] Woods, R. J., & Pikaev, A. K. (1994). *Applied Radiation Chemistry: Radiation Processing*. New York: Wiley.

[26] AMERICAN ELEMENTS® | The Advanced Materials Manufacturer. (n.d.). Retrieved March 5-7, 2019, from https://www.americanelements.com/

A

List of Chemicals, Equipment and Software

A.1 Chemicals

List of chemicals used:

- Cerium(III) chloride heptahydrate, $CeCl_3 \bullet 7H_2O$
- Copper(II) sulfate pentahydrate, $CuSO_4 \bullet 5H_2O$
- Gadolinium(III) chloride hexahydrate, $GdCl_3 \bullet 6H_2O$
- Iron(II) sulfate heptahydrate, $FeSO_4 \bullet 7H_2O$
- Lead(II) nitrate, $Pb(NO_3)_2$
- Lubriseal Stopckock Grease
- Milli-Q water, H_2O
- Sodium chloride, $NaCl$
- Sulfuric acid, H_2SO_4
- Ytterbium(III) chloride hexahydrate, $YbCl_3 \bullet 6H_2O$

A.2 Equipment

List of equipment used:

- 1ml plastic bulb pipette
- 100ml volumetric flask
- 1000ml volumetric flask
- 2ml plastic bulb pipette
- 20ml glass vials
- 200ml glass beaker
- 5ml pipette tips
- 50ml plastic vials
- 50ml glass beaker
- 50ml volumetric flask
- Gammacell 220
- Jacketed beaker
- Lambda 25 UV/VIS spectrometer
- Large plastic measuring tray
- Metal measuring spoon
- Mettler Toledo 5ml pipette
- Mettler Toledo level balances

- Plastic beakers with lids
- 10mm Quarts cuvettes
- Self made plastic coil
- Small plastic measuring tray

A.3 Software

List of software used:

- MATLAB ® 9.5.0.944444 (R2018b)
- Microsoft ® Visio ® 2016 MSO (16.0.10730.20264) 32-bit
- Microsoft ® Excel ® 2013 (15.0.5127.1000) MSO (15.0.5127.1000) 32-bit
- PerkinElmer UV WinLab ® 2002-2012 6.3.1.0748

B

Previous dosimetry measurement

Figure (B.1) and (B.2) presents the results from dosimetry measurements preformed 19.04.2012 by Ivan Kajan, in connection with his PhD thesis, Transport and Containment Chemistry of Ruthenium under Severe Accident Conditions in a Nuclear Power Plant.

Figure B.1: Results from measurements preformed by Ivan Kajan 19.04.2012.

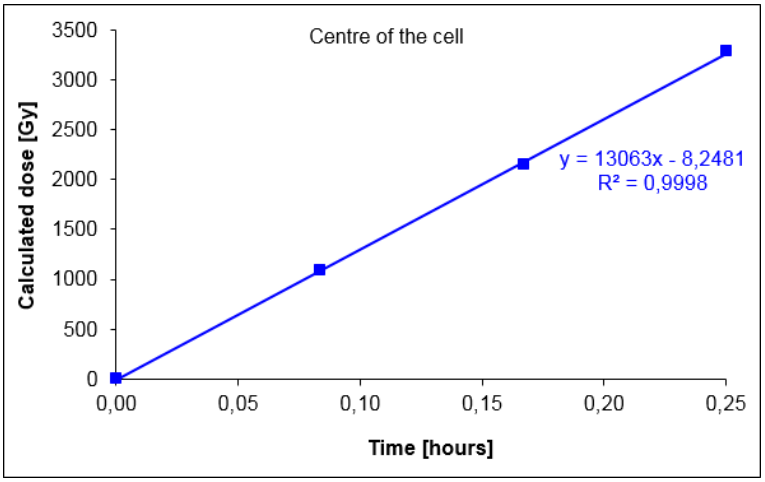

Figure B.2: Results from measurements preformed by Ivan Kajan 19.04.2012.

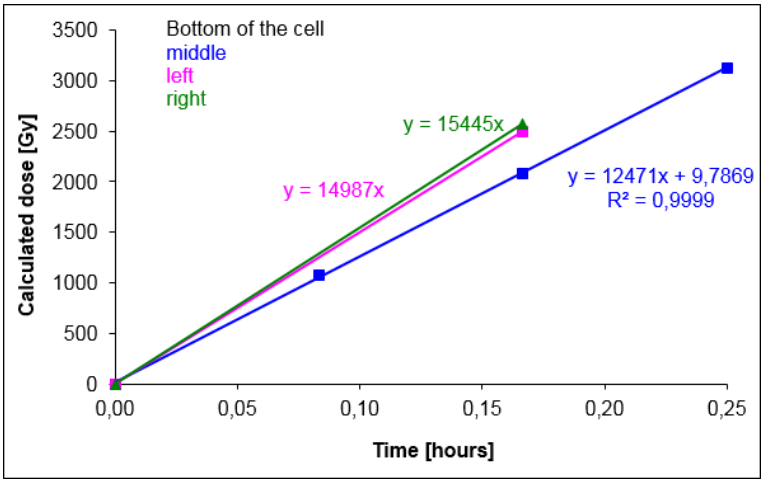

The present day dose is estimated by using equation (3.5), found under chapter 3.1 Equations, and by relating absorbed dose to activity. Present day for these calculations was set to 19.04.2019, which was a few days prior to the first experiment.

- Center of the cell
  - Middle $D \approx 5205Gy$
- Bottom of the cell
  - Middle $D \approx 4969Gy$
  - Left $D \approx 5972Gy$
  - Right $D \approx 6153Gy$